Nanoscale Horizons
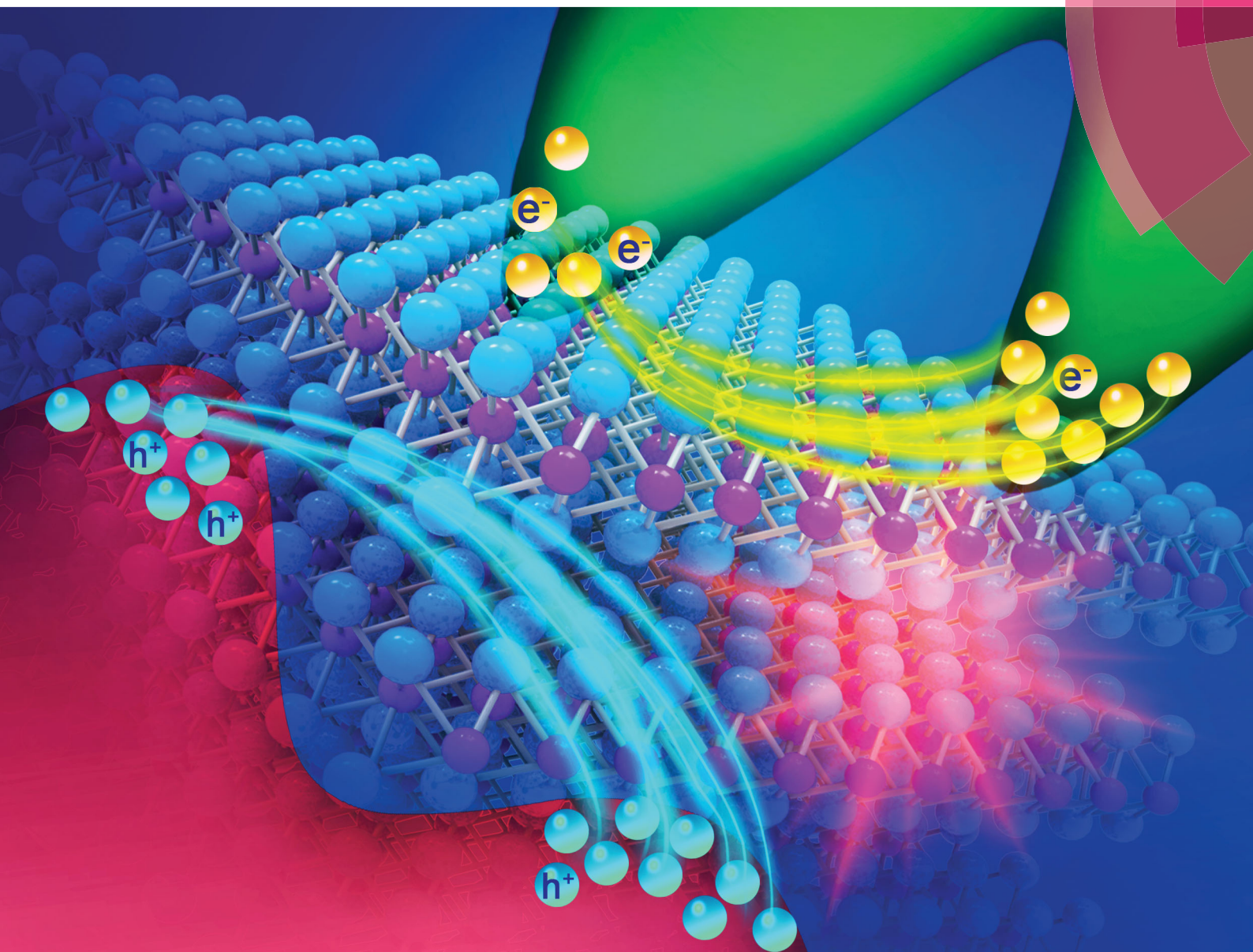
The home for rapid reports of exceptional significance in nanoscience and nanotechnology

rsc.li/nanoscale-horizons

ROYAL SOCIETY OF CHEMISTRY

NCNST

COMMUNICATION
Weizhen Liu, Haiyang Xu *et al.*
High-temperature driven inter-valley carrier transfer and significant fluorescence enhancement in multilayer WS$_2$

Check for updates

High-temperature driven inter-valley carrier transfer and significant fluorescence enhancement in multilayer WS$_2$†

Heyu Chen,[a] Yuanzheng Li,[a] Weizhen Liu,*[ab] Haiyang Xu, [ID] *[a] Guochun Yang, [ID] [a] Jia Shi,[c] Qiushi Feng,[a] Tong Yu,[a] Xinfeng Liu [ID] [c] and Yichun Liu[a]

It is quite necessary to understand and control the essential carrier dynamic behaviors of two-dimensional WS$_2$, which is regarded as a very promising material for integrated nanoelectronic and opto-electronic devices. Herein, a high-temperature driven carrier transfer process of multilayer WS$_2$ nanoflakes is proposed. The established model, involving the inter-valley transfer process of photocarriers from the Λ/Γ point to the K point, predicts the significant emission enhancement of the $K \rightarrow K$ direct transition at high temperatures, which is verified by both theoretical calculations and experimental observations. On the one hand, variations in the estimated population ratio of photo-carriers with increasing temperature well support the proposed model. On the other hand, temperature-dependent photoluminescence spectra clearly show that the $K \rightarrow K$ direct emission intensity is remarkably enhanced by ~300-fold as the temperature is elevated to 760 K. Time-resolved fluorescence spectral studies confirm the occurrence of the inter-valley carrier transfer process in the multilayer WS$_2$. These results provide solid evidence for the proposed inter-valley carrier transfer model. Such a mechanism could not only be applied to improve the luminescence intensity of indirect-band-gap semiconductors, but also be further extended to design optoelectronic devices which have special requirements on controlling the carrier dynamic behavior.

Conceptual insights

Transition metal dichalcogenides (TMDs) hold great promise for technological applications in the fields of nanoelectronics and optoelectronics, owing to their superior electronic and optical properties. Multilayer TMDs have many notable superiorities over their monolayer counterparts such as higher electron mobility, stronger photon absorption ability and larger optical density of states. Therefore, it is essentially important to improve the optical performance of ML-TMDs and understand their excited-state carrier dynamics, which may pave the way for future exploration of ML-TMD-based optoelectronic devices. However, research reports on ML-TMDs are relatively rare in comparison with those on their monolayer counterparts. Herein, a remarkable high-temperature-induced fluorescence emission enhancement (~300-fold) from ML-WS$_2$ nanoflakes is observed for the first time. A theoretical model involving thermo-driven inter-valley transfer of photocarriers is proposed that explains this intriguing phenomenon. Population ratio calculations and multiple spectral characterization (temperature-dependent and time-resolved spectra) confirm the validity and reliability of this established inter-valley transfer model. The present study not only suggests a general strategy to enhance the luminescence performance of indirect-band-gap semiconductors but also sheds more light on the carrier dynamic mechanism of 2D materials, both of which are very important to develop new-type electronic and photonic devices based on these emerging materials.

Introduction

Transition metal dichalcogenides (TMDs) hold great promise for technological applications in various fields including

tunneling transistors, photodetectors, LEDs and flexible electronics, owing to their superior electronic and optical properties.[1–8] Among them, MoS$_2$, as a typical representative for TMDs, has attracted the most attention due to its relatively easy availability through mechanical exfoliation or chemical vapor deposition. On the other hand, closely related WS$_2$ is quickly attracting extensive interest as well.[5–11] Recently, WS$_2$ with a similar layered structure to MoS$_2$ has been found to exhibit a finite band-gap in the visible wavelength range.[3,11–13] In addition, compared with MoS$_2$, monolayer WS$_2$ has a superior luminescence quantum efficiency and a larger spin–orbit coupling strength, suggesting that it may exhibit larger band edge splitting and a stronger magnetic coupling effect.[5,6,14–17] These merits could lead to the realization of high-performance

a Centre for Advanced Optoelectronic Functional Materials Research and Key Laboratory of UV-Emitting Materials and Technology (Northeast Normal University), Ministry of Education, Changchun 130024, China. E-mail: hyxu@nenu.edu.cn

b National Demonstration Center for Experimental Physics Education (Northeast Normal University), Changchun 130024, China. E-mail: wzliu@nenu.edu.cn

c Division of Nanophotonics, CAS Key Laboratory of Standardization and Measurement for Nanotechnology, CAS Center for Excellence in Nanoscience, National Center for Nanoscience and Technology, Beijing 100190, China

† Electronic supplementary information (ESI) available. See DOI: 10.1039/c8nh00123e

optoelectronic and spintronic devices based on two-dimensional (2D) WS$_2$ materials.[17–19]

It should be noted that the optical properties of TMDs vary significantly with layer thickness.[11,13] Monolayer WS$_2$ is a direct band-gap semiconductor with a band-gap value of ~ 2.0 eV. However, it exhibits an indirect band-gap of ~ 1.4 eV in the multilayer (ML) configuration and shows a markedly suppressed fluorescence quantum yield.[9,15] Obviously, the indirect-band-gap nature of ML-TMDs limits their applications in optoelectronic devices such as LEDs, photodetectors and lasers. In fact, ML samples have many notable superiorities over their monolayer counterparts such as higher electron mobility, stronger photon absorption ability and larger optical density of states.[20–22] Therefore, it is essentially important to improve the optical performance of ML-TMDs and understand their excited-state carrier dynamics, which may pave the way for future exploration of ML-TMD-based optoelectronic devices. However, research reports on the ML-TMDs are relatively rare in comparison with those on their monolayer counterparts.

In this work, the high-temperature carrier dynamics of ML-WS$_2$ have been theoretically studied according to the Boltzmann distribution law. The population ratio of electrons and holes in different energy valleys and hills and its variation with increasing temperature are carefully examined. Furthermore, a significant fluorescence emission enhancement at high temperatures is expected on the basis of these theoretical analyses, and is indeed observed for the first time in subsequent temperature-dependent PL experiments. Time-resolved spectral measurements confirm that high-temperature-induced inter-valley transfer of photocarriers should be responsible for the observed PL variations. The current research not only provides an effective method for improving the luminescence performance of indirect-band-gap ML-TMDs, but also deepens the understanding of the excited-state carrier dynamics in the TMD material family.

Results and discussion

Fig. 1(a) illustrates the ball-and-stick structural model of a ML-WS$_2$ nanoflake. Each molecular layer comprises two hexagonal planes of S atoms and an intermediate hexagonal plane of W atoms. The W atoms coordinate with the S atoms through ionic–covalent bond interactions in a trigonal prismatic manner.[11,23] Environmental temperature has a huge impact on the physical properties of semiconductors. In general, the number of phonons will increase due to stronger lattice vibrations with increasing temperature, which may induce some intriguing carrier dynamic behaviors and optical phenomena. Therefore, heating is usually considered as a simple and efficient strategy to tune the optical
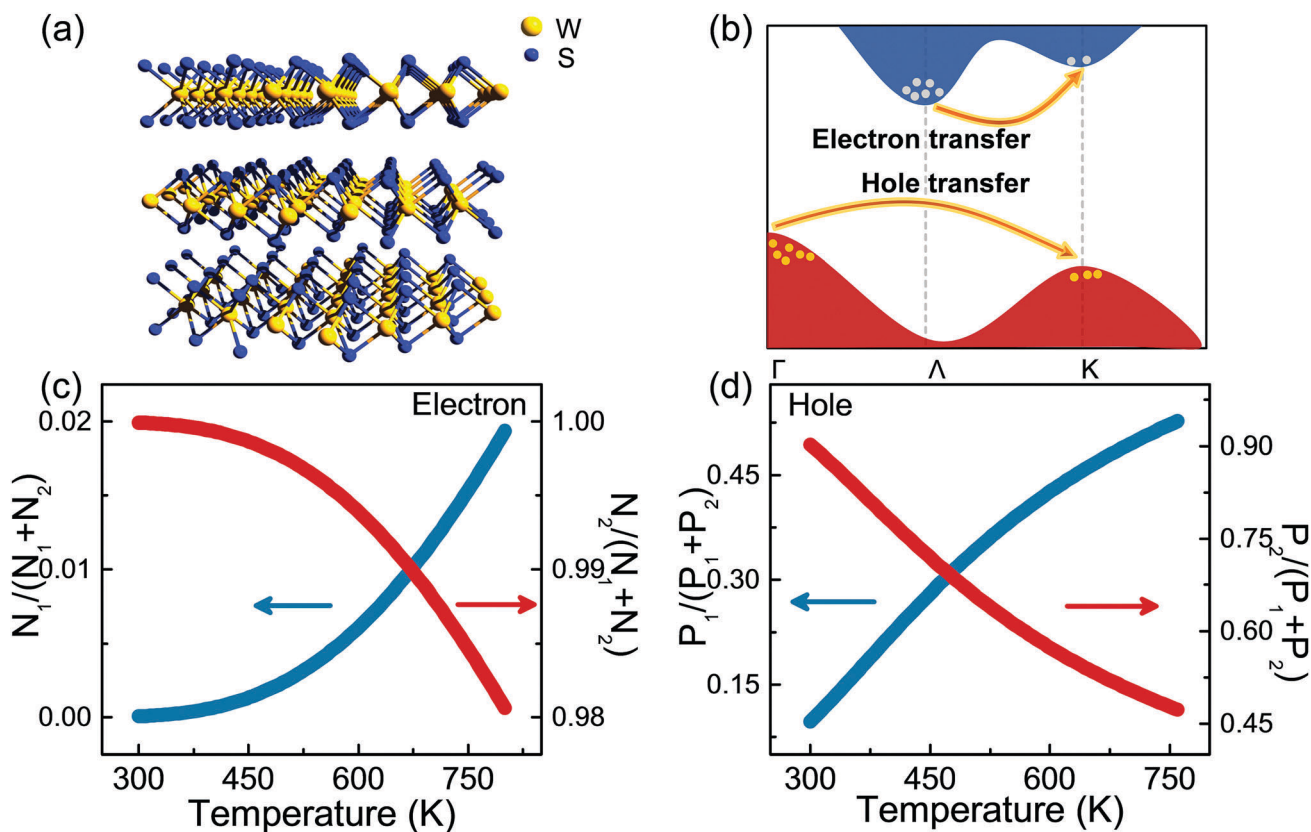

Fig. 1 (a) Structural schematic diagram of a multilayer 2H-WS$_2$ sample. (b) A scheme showing the transfer process of photo-carriers among different energy valleys and hills; the orange arrows indicate the transfer direction from Λ/Γ to K. Population ratio of the electrons (c) and holes (d) in the K point (blue curve) and the Λ/Γ point (red curve) as a function of the measurement temperature in ML-WS$_2$.

properties of materials. In the current case, a high-temperature-driven carrier transfer process, termed as inter-valley transfer of photo-carriers, is expected to occur in the ML-WS$_2$ sample. Fig. 1(b) illustrates the specific carrier transfer process in the energy band diagram of a ML-WS$_2$ nanoflake. It has been proved that conduction band valleys of ML-WS$_2$ are located at the Λ and K points of the Brillouin zone, while valence band hills are located at the Γ and K points.[3,23,24] In particular, the conduction band minimum (CBM) and valence band maximum (VBM) of ML-WS$_2$ are respectively situated at the Λ valley for electrons and the Γ hill for holes, indicating the indirect-band-gap feature of ML-WS$_2$. Therefore, most photo-carriers would occupy the Λ valley and the Γ hill at room temperature. However, when the temperature increases, excited-state electrons and holes will gain extra energy from the surrounding crystal lattices as a result of the intensified carrier–phonon interaction.[25] Thus, as indicated by the orange arrows in Fig. 1(b), the electrons obtaining sufficient kinetic energy will transfer from the Λ valley to the K valley, while the holes with greatly improved kinetic energy will also experience a similar transfer from the Γ hill to the K hill. Through this process, more electrons and holes will occupy the K valley and the K hill at high temperatures.

In order to verify this proposed transfer model, both theoretical analyses and experimental studies have been carried out. First, a rough estimation of the temperature-dependent carrier population ratio among different energy valleys and hills is conducted according to the Boltzmann distribution law. The relevant results are illustrated in Fig. 1(c) and (d) (see Note 1 of the ESI† for calculation details). It could be seen in Fig. 1(c) that the population ratio of the electrons at the K valley $N_1/(N_1 + N_2)$ (herein, N_1 and N_2 correspond to the electron numbers at the K valley and Λ valley, respectively) shows a rapid increasing trend as the temperature increases. In contrast, the electron

occupation ratio at the Λ valley $N_2/(N_1 + N_2)$ decreases monotonously with increasing temperature. Similarly, the population ratio of the holes at the K hill $P_1/(P_1 + P_2)$ increases, whereas that at the Γ hill $P_2/(P_1 + P_2)$ declines when the temperature is elevated (see Fig. 1(d); P_1 and P_2 stand for the hole numbers at the K hill and Γ hill, respectively). More specifically, the above estimations demonstrate that the population ratio of photo-carriers at the K point (including the K-valley and K-hill) is improved $\sim$1000-fold when the environmental temperature is increased from 300 to 760 K. The opposite change tendency of the population ratio at the K point and the Λ/Γ point implies that inter-valley carrier transfer could occur theoretically as the temperature continuously increases. In such a case, the number of excited-state carriers at the K point will be largely increased, which may significantly enhance the emission intensity of the $K \rightarrow K$ direct transition of ML-WS$_2$.

To experimentally examine whether the fluorescence emission intensity of ML-WS$_2$ is improved or not, temperature-dependent PL (TD-PL) measurements from 300 to 760 K are performed for mechanically exfoliated ML-WS$_2$ flakes. Fig. 2(a) shows an atomic force microscopy (AFM) image of an exfoliated ML-WS$_2$ flake with a thickness of $\sim$18.5 nm, corresponding to $\sim$23 layers. To prevent the sample from being oxidized at high temperatures, high-purity argon is employed as a shielding gas during the whole PL measurement procedure. Fig. 2(b) shows the TD-PL spectra of this ML-WS$_2$ sample. As an indirect-band-gap semiconductor, the PL intensity of ML-WS$_2$ is usually very low. Only a weak emission peak with a broad linewidth is observed at $\sim$870 nm when the temperature is below 400 K.

This weak PL signal can be attributed to the indirect-band-gap transitions in ML-WS$_2$, because indirect emissions generally show very low quantum yields.[26] As the measurement temperature increases to 440 K, another PL peak appears at $\sim$690 nm,
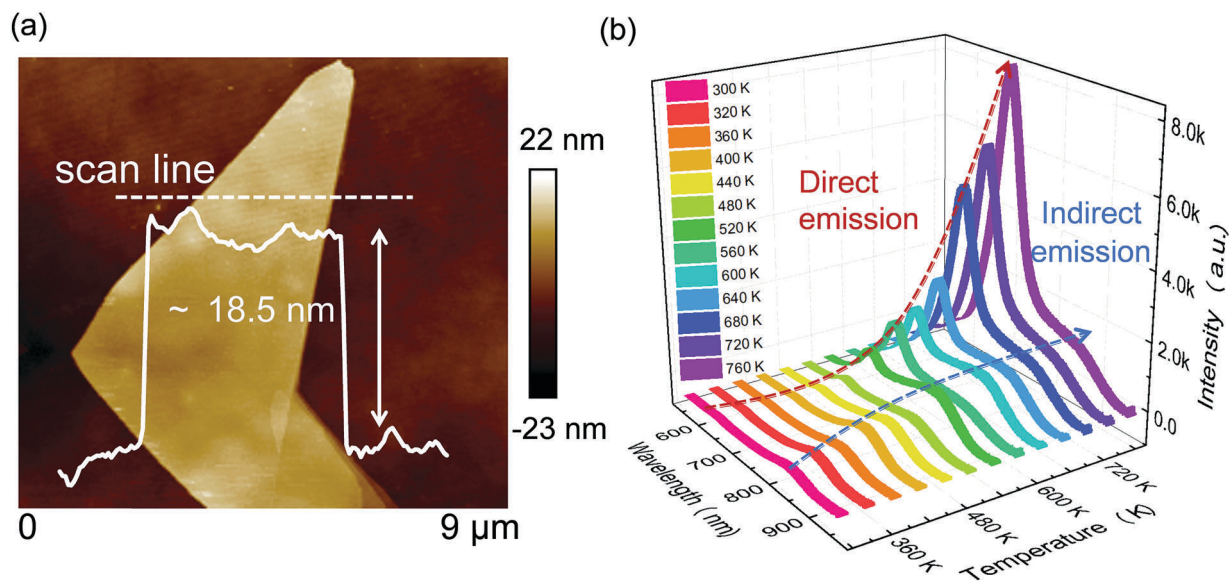

Fig. 2 (a) A typical AFM image showing the height profile of the mechanically exfoliated ML-WS$_2$ flake. (b) Steady-state TD-PL spectra of the ML-WS$_2$ sample taken at a temperature range of 300–760 K; the red and blue dashed arrows respectively indicate the variations of direct and indirect emission peaks with temperature.
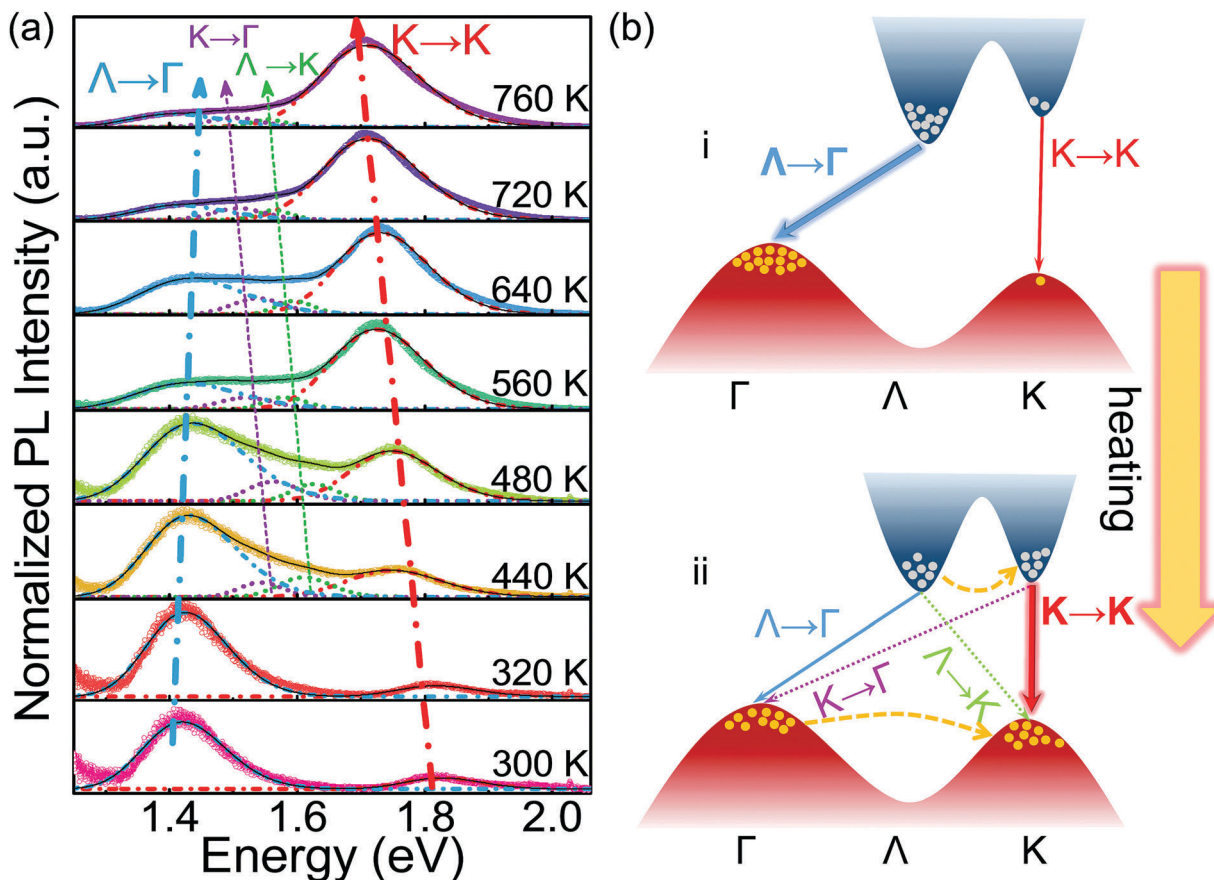
Fig. 3 (a) Multi-peak deconvolution fittings of the TD-PL spectra, showing the specific variation of each sub-peak at different temperatures. (b) Schematic diagram illustrating the excited-state carrier distribution and possible radiative transition routes at (i) room temperature and (ii) high temperature; the carrier population at the K point is effectively increased due to the heat-induced inter-valley transfer process in panel (ii).

corresponding to the $K \rightarrow K$ direct transition emission of ML-WS$_2$. The above assignments of the PL peaks will be discussed in detail in Fig. 3. Further increasing the temperature leads to the PL intensity improvement for both peaks, but the short-wavelength direct emission shows a more rapid increase rate than the long-wavelength indirect emission. After 560 K, the PL intensity of the direct emission is higher than that of the indirect emission. The entire PL spectrum is dominated by the direct emission at a high temperature of 760 K. To avoid the thermo-induced sample destruction or defect formation caused by atom evaporation, the measurement temperature is not further elevated. The TD-PL spectra of other ML-WS$_2$ samples with different thicknesses are also tested, and similar high-temperature-induced fluorescence emission enhancements are observed (see Fig. S1 of the ESI†), confirming the reliability and reproducibility of this intriguing luminescence phenomenon.

It is noteworthy that the vast majority of previous reports on 2D materials mainly focus on monolayer or few-layer (*e.g.* bilayer or trilayer) flakes, which are usually grown by chemical vapor deposition or other physical/chemical methods. Herein, we pay attention to the luminescence properties of multilayer (> 10-layer) WS$_2$ samples with different thicknesses. To easily obtain these multilayer samples, a simple mechanical exfoliation method is adopted. Honestly speaking, the mechanical exfoliation approach

does not have good control over the sample thickness. However, it is still able to produce experimental specimens with large thickness difference *via* a multi-cycle peeling process. In the current work, three multilayer WS$_2$ flakes with distinctly different thicknesses of 18.5 nm (~ 23-layer and < 50-layer), 54 nm (~ 68-layer and > 50-layer) and 120 nm (~ 150-layer and > 100-layer) are intentionally created, to confirm that the heating-triggered luminescence enhancement phenomenon could happen in multilayer WS$_2$ samples with distinctly different thicknesses. As expected, similar fluorescence emission enhancements at elevated temperatures are observed (see Fig. S1 of the ESI†), indicating the validity of the proposed inter-valley carrier transfer model for multilayer WS$_2$ samples.

For better analyzing these TD-PL spectra, Gaussian deconvolution multi-peak fittings are performed, and the relevant results are shown in Fig. 3(a). As can be seen, all spectra are mainly composed of two emission bands at different measurement temperatures. One is the indirect transition emission located at ~ 1.42 eV at 300 K, originating from the $\Lambda \rightarrow \Gamma$ transition (see Fig. 3(b)). The other is the direct transition emission situated at ~ 1.82 eV at 300 K, stemming from the $K \rightarrow K$ direct recombination. At a relatively low temperature of 300 K, the PL intensity of the $\Lambda \rightarrow \Gamma$ indirect emission is obviously higher than that of the $K \rightarrow K$ direct emission. This is

because ML-WS$_2$ is an indirect-band-gap semiconductor. Nearly all photo-excited electrons and holes are respectively populated at the CBM (Λ valley) and the VBM (Γ hill) at room temperature. Therefore, only the $\Lambda \rightarrow \Gamma$ indirect emission can be observed, whereas the $K \rightarrow K$ direct emission, with a just detectable intensity, is extremely weak. With the increase of measurement temperature, the $K \rightarrow K$ emission intensity improves quickly and exceeds the $\Lambda \rightarrow \Gamma$ emission intensity at 560 K. At 760 K, the $K \rightarrow K$ direct emission peak dominates over the entire PL spectrum. As analyzed above, high temperatures induce a re-distribution of photo-carriers. More electrons and holes are transferred from the Λ/Γ point to the K point, which increases the carrier population fraction at the K point and thus enhances the $K \rightarrow K$ direct emission intensity.

It is noted in Fig. 3(a) that two additional K-point-related emission peaks ($K \rightarrow \Gamma$ transition and $\Lambda \rightarrow K$ transition, see Fig. 3(b)) are also activated at high temperatures owing to the increased K-point population ratio. In fact, the emergence of these two new peaks could be just viewed as a piece of clear evidence for the proposed carrier transfer model. Besides, the red shifts of the emission energy for the K-point-related transitions ($K \rightarrow K$, $K \rightarrow \Gamma$ and $\Lambda \rightarrow K$) are observed as the temperature rises. This is a common result for the TD-PL spectra of semiconductor materials, and could be attributed to the thermo-induced band-gap shrinkage effect.[27–29] In the current case, the K valley moves downward and the K hill moves upward, reducing the K-point-related band-gap and emission energy at high temperatures.[24,27] However, an interesting finding is that the $\Lambda \rightarrow \Gamma$ indirect transition displays an anomalous blue shift in emission energy. According to a previous theoretical calculation study,[24] this may be because the Λ valley and the Γ hill would slightly depart from each other (upshift for the Λ valley, while downshift for the Γ hill) with increasing temperature. Such a variation will slightly enlarge the band-gap between the Λ valley and the Γ hill, resulting in a small increment in the $\Lambda \rightarrow \Gamma$ emission energy. A similar high-temperature causing a blue-shift phenomenon of the $\Lambda \rightarrow \Gamma$ transition in other TMDs has also been observed by Zhao *et al.*[24]

To clearly demonstrate the enhancement extent of the two main emissions, Fig. 4(a) shows the specific enhancement factor (F_E) of the $K \rightarrow K$ direct and $\Lambda \rightarrow \Gamma$ indirect transitions at different temperatures. Herein, the enhancement factor F_E is defined as the ratio between the $K \rightarrow K$ (or $\Lambda \rightarrow \Gamma$) emission intensity (integrated) at elevated temperatures and that at room temperature. As is shown, a remarkable enhancement is observed for the $K \rightarrow K$ direct emission intensity by increasing the measurement temperature, and a ~300-fold F_E is obtained at 760 K. In contrast, the $\Lambda \rightarrow \Gamma$ indirect emission exhibits a negligible PL enhancement. The derived F_E for the $\Lambda \rightarrow \Gamma$ emission is merely one percent of the enhancement factor for the $K \rightarrow K$ direct emission. This minute improvement of the $\Lambda \rightarrow \Gamma$ emission intensity could be ascribed to the strengthened electron–phonon (or electron–lattice) interaction at elevated temperatures, which facilitates the phonon-assisted indirect radiative transition.[30,31] Fig. 4(b) shows the temperature dependence of the integrated intensity ratio of the $K \rightarrow K$
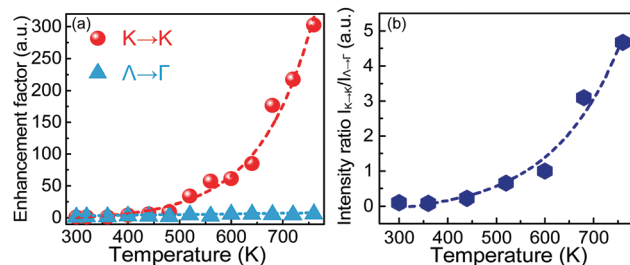

Fig. 4 (a) Enhancement factor of the $K \rightarrow K$ direct and $\Lambda \rightarrow \Gamma$ indirect emissions at different temperatures. (b) Temperature dependence of the integrated intensity ratio of the $K \rightarrow K$ direct emission to the $\Lambda \rightarrow \Gamma$ indirect emission ($I_{K \rightarrow K}/I_{\Lambda \rightarrow \Gamma}$).

direct emission to the $\Lambda \rightarrow \Gamma$ indirect emission ($I_{K \rightarrow K}/I_{\Lambda \rightarrow \Gamma}$), which can reflect the relative intensity variation of these two luminescent components. As can be seen, the $I_{K \rightarrow K}/I_{\Lambda \rightarrow \Gamma}$ value demonstrates a monotonous increasing trend with temperature, indicating a much faster PL intensity increase rate of the $K \rightarrow K$ direct emission than that of the $\Lambda \rightarrow \Gamma$ indirect emission. This is consistent with the former analysis, further confirming the validity of our proposed carrier transfer mechanism. Herein, a comparison of the radiative recombination probability at the K point (P_K) and the Λ/Γ point ($P_{\Lambda/\Gamma}$) is made on the basis of the $I_{K \rightarrow K}/I_{\Lambda \rightarrow \Gamma}$ value at 760 K (see Note 2 of the ESI† for detailed discussion). This comparison suggests that the P_K of the K-point-related direct transition is generally one to two orders of magnitude higher than the $P_{\Lambda/\Gamma}$ of Λ/Γ-point-related indirect transitions, verifying the effectiveness of the $K \rightarrow K$ direct transition as a high-efficiency radiative recombination channel.

Fig. 5(a) shows the time-resolved PL spectra of the $K \rightarrow K$ direct emission at different temperatures, which can directly reflect the temperature-dependent exited-state carrier dynamic process. As is shown, all transient-state spectra demonstrate a similar decay behavior with time, and could be well fitted by an exponential attenuation function: $I = A \exp(-t/\tau) + I_0$. Herein, τ is the effective lifetime of the K-point photo-carriers; A and I_0 are two fitting parameters (see Note 3 of the ESI† for detailed fitting results). As can be deduced from the fitting equation, I is equal to I_0 as the time τ approaches infinity. From this point of
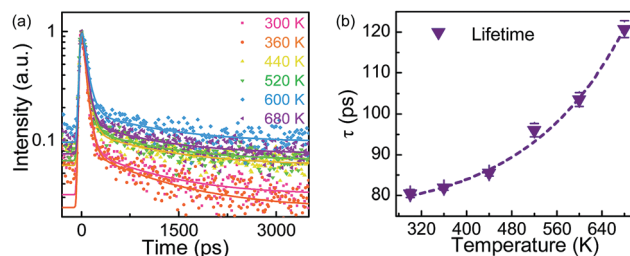

Fig. 5 (a) Time-resolved PL spectra of the $K \rightarrow K$ direct emission at different temperatures. The solid lines are exponential decay fittings of the obtained experimental data points, giving out the effective fluorescence lifetime of the $K \rightarrow K$ direct emission. (b) The fitted effective lifetime τ as a function of the measurement temperature.

view, the fitting parameter I_0 represents the residual fluorescence background signal after the effective emission intensity completely decays. The residual fluorescence background signal may come from the testing instrument response or ambient environment noise. Usually, the excited-state carriers can decay through both radiative (*e.g.* excitons/electron–hole-pairs radiative emission) and non-radiative (*e.g.* carrier–carrier scattering-induced Auger process or carrier–phonon scattering-induced lattice heating effect) recombination pathways.[32–34] Hence, the τ derived here represents the overall depopulation situation of the K point carriers induced by the above radiative and non-radiative factors. Fig. 5(b) illustrates the variation trend of the τ value as a function of the measurement temperature. As can be seen, the τ value is ~ 80 ps at 300 K, which is in good agreement with the reported carrier lifetime value in 2D WS$_2$ materials.[35,36] It is generally believed that the excited-state lifetime of semiconductors will decrease with increasing temperature, as a result of the strengthened carrier–phonon/carrier–carrier interactions or more thermally-activated non-radiative channels.[37,38] However, it is observed that τ exhibits an abnormal uptrend from ~ 80 to ~ 120 ps when the measurement temperature is elevated from 300 to 680 K, which is inconsistent with the previous cognition. In fact, such an abnormal lifetime increase of the K point carriers could just prove the occurrence of inter-valley transfer at high temperatures, which shall be interpreted as follows. According to the proposed model, photo-carriers would transfer from the Λ/Γ point to the K point at elevated temperatures. Thanks to this transfer process, the K point carrier number is supplemented effectively and timely by these "newly injected" carriers from the Λ/Γ point, leading to the observed elongated lifetime of the K point carriers. In addition, because a considerable amount of these "newly injected" carriers participate in the radiative recombination process, the PL intensity of the $K \to K$ direct transition is significantly enhanced with increasing temperatures. Although the transient-state fluorescence characterization is unable to be performed on the $\Lambda \to \Gamma$ indirect emission due to the limited detection wavelength (300–800 nm) of the current spectroscopy system, the current experimental observations of the enhanced $K \to K$ emission intensity and the prolonged K-point excited-state lifetime at elevated temperatures have provided solid support to the proposed inter-valley carrier transfer model.

One may argue that the thermal expansion induced interlayer decoupling effect can switch the band-gap structure of ML-WS$_2$ from indirect transition to direct transition, and thus improve its PL intensity.[27] However, such a scenario cannot happen in the current case because of the extremely small thermal expansion coefficient of the ML-WS$_2$ sample. The estimated increment in the c-axis interlayer distance (Δd) is ~ 0.005 Å at 760 K, which is far less than the necessary Δd of ~ 0.97 Å for the occurrence of indirect-to-direct band-gap switching in ML-WS$_2$. As for the in-plane a-axis thermal expansion, its Δd is also very small (~ 0.009 Å) and has almost no impact on the band-gap structure of ML-WS$_2$. Detailed calculations and analyses of the thermal expansion induced band-gap structure

evolution in ML-WS$_2$ have been shown in Fig. S2–S4 and Note 4 of the ESI.† In addition, the bandgap structure evolution of ML-WS$_2$ with different layer numbers has also been calculated and discussed in Fig. S5 of the ESI.† On the basis of the above discussion, it is concluded that the thermal expansion induced interlayer decoupling cannot be the main cause responsible for the high-temperature fluorescence enhancement observed in ML-WS$_2$.

Another plausible explanation for the high-temperature induced PL improvement is the formation of more defects (*e.g.* sulfur vacancies) after the thermal annealing process.[39] To rule out this factor, PL and Raman spectra of this ML-WS$_2$ sample are measured before and after the TD-PL test (see Fig. S6 of the ESI†). As can be seen, the PL and Raman spectra before/after the TD-PL test look almost the same. No obvious peak broadening or wavelength shift occurs, suggesting that there is no notable defect multiplication after the TD-PL test. Therefore, the observed PL variation is not induced by the formation of more defects. In addition, the thickness of the ML-WS$_2$ flake before/after the TD-PL test is nearly unchanged (see Fig. S7 of the ESI†), indicating that the PL enhancement is not improved by the sample thickness change either. Finally, the effects of different supporting substrates and laser excitation power on the PL behavior of ML-WS$_2$ are also studied and discussed in detail (see Fig. S8 and S9 of the ESI†). It is found that the substrate effect (*e.g.* interfacial strain, lattice mismatch or charge transfer between the substrate and the sample) or laser effect (*e.g.* power fluctuation, local heating or sample damage) is not the main cause for the observed fluorescence emission enhancement at high temperatures.

Experimental section

ML-WS$_2$ flakes were mechanically exfoliated from a WS$_2$ bulk crystal (SPI Supplies Inc.), and then transferred onto commercially available SiO$_2$/Si substrates (the SiO$_2$ layer is ~ 300 nm) for subsequent research. AFM (Bruker Dimension® Icon™) was employed to study the surface topography and sample thickness of these ML-WS$_2$ flakes. A JY HR-800 LabRam Infinity Spectrophotometer, equipped with a 488 nm laser as the excitation source and a Si photodiode as the signal detector, was employed to measure the steady-state PL and Raman spectra. The laser output power is fixed at ~ 1 mW during the temperature-dependent PL measurements, and the laser spot size is focused to be ~ 0.5 μm. Thus, the laser power density is ~ 4 mW μm^{-2}. A time-correlated single-photon counting technique (TCSPC, B&H Company) was used to record the time-resolved PL spectra of the ML-WS$_2$ samples. The corresponding excitation light source for the TR-PL test is a 530 nm laser generated from a Mira 900 oscillator pulsed laser source with a repetition rate of 76 MHz and a pulse width of 120 fs. An electric heater (Linkam, TMS 600), equipped with an argon gas blower (preventing the samples from being oxidized at high temperatures), was adopted to heat the ML-WS$_2$ flakes for temperature-dependent PL (including steady-state and transient-state) and Raman characterization.

Conclusions

In summary, a hot-carrier dynamic model is established based on the high-temperature driven inter-valley transfer mechanism of excited-state carriers among different energy valleys and hills. Significant fluorescence emission enhancement deduced from this model is indeed observed in the ML-WS$_2$ nanoflake for the first time. Population ratio calculations and multiple spectral characterization techniques (including TD-PL and TR-PL) confirm the validity and reliability of this established inter-valley transfer model. The present study not only suggests an efficient strategy to enhance the luminescence performance of indirect-band-gap ML-TMDs, but also sheds more light on the carrier dynamic mechanism (e.g. transfer, relaxation, scattering, and recombination) of 2D materials, both of which are very important to develop new-type electronic and photonic devices based on these emerging materials.

Conflicts of interest

There are no conflicts to declare.

Acknowledgements

References

1 W. Choi, N. Choudhary, G. H. Han, J. Park, D. Akinwande and Y. H. Lee, *Mater. Today*, 2017, **20**, 116–130.

2 S. Manzeli, D. Ovchinnikov, D. Pasquier, O. V. Yazyev and A. Kis, *Nat. Rev. Mater.*, 2017, **2**, 17033.

3 Q. H. Wang, K. Kalantar-Zadeh, A. Kis, J. N. Coleman and M. S. Strano, *Nat. Nanotechnol.*, 2012, **7**, 699–712.

4 H. Li, J. Wu, Z. Yin and H. Zhang, *Acc. Chem. Res.*, 2014, **47**, 1067–1075.

5 K. M. McCreary, A. T. Hanbicki, G. G. Jernigan, J. C. Culbertson and B. T. Jonker, *Sci. Rep.*, 2016, **6**, 19159.

6 M. Samadi, N. Sarikhani, M. Zirak, H. Zhang, H. Zhang and A. Z. Moshfegh, *Nanoscale Horiz.*, 2018, **3**, 90–204.

7 M. L. Tsai, M. Y. Li, Y. Shi, L. J. Chen, L. J. Li and J. H. He, *Nanoscale Horiz.*, 2017, **2**, 37–42.

8 M. Z. Bellus, M. Li, S. Lane, F. Ceballos, Q. Cui, X. C. Zeng and H. Zhao, *Nanoscale Horiz.*, 2017, **2**, 31–36.

9 A. Splendiani, L. Sun, Y. Zhang, T. Li, J. Kim, C.-Y. Chim, G. Galli and F. Wang, *Nano Lett.*, 2010, **10**, 1271–1275.

10 J. K. Ellis, M. J. Lucero and G. E. Scuseria, *Appl. Phys. Lett.*, 2011, **99**, 261908.

11 K. F. Mak, C. Lee, J. Hone, J. Shan and T. F. Heinz, *Phys. Rev. Lett.*, 2010, **105**, 136805.

12 M. Chhowalla, H. S. Shin, G. Eda, L.-J. Li, K. P. Loh and H. Zhang, *Nat. Chem.*, 2013, **5**, 263–275.

13 R. Dhall, M. R. Neupane, D. Wickramaratne, M. Mecklenburg, Z. Li, C. Moore, R. K. Lake and S. Cronin, *Adv. Mater.*, 2015, **27**, 1573–1578.

14 P. Tonndorf, R. Schmidt, P. Böttger, X. Zhang, J. Börner, A. Liebig, M. Albrecht, C. Kloc, O. Gordan, D. R. T. Zahn, S. Michaelis de Vasconcellos and R. Bratschitsch, *Opt. Express*, 2013, **21**, 4908–4916.

15 K. Kośmider and J. Fernández-Rossier, *Phys. Rev. B: Condens. Matter Mater. Phys.*, 2013, **87**, 075451.

16 Z. Y. Zhu, Y. C. Cheng and U. Schwingenschlögl, *Phys. Rev. B: Condens. Matter Mater. Phys.*, 2011, **84**, 153402.

17 P. R. Pudasaini, A. Oyedele, C. Zhang, M. G. Stanford, N. Cross, A. T. Wong, A. N. Hoffman, K. Xiao, G. Duscher, D. G. Mandrus, T. Z. Ward and P. D. Rack, *Nano Res.*, 2017, **11**, 722–730.

18 Y. Wen, Y. Xia and S. Zhang, *J. Power Sources*, 2016, **307**, 593–598.

19 S. Jo, N. Ubrig, H. Berger, A. B. Kuzmenko and A. F. Morpurgo, *Nano Lett.*, 2014, **14**, 2019–2025.

20 Y. Li, H. Xu, W. Liu, G. Yang, J. Shi, Z. Liu, X. Liu, Z. Wang, Q. Tang and Y. Liu, *Small*, 2017, **13**, 1700157.

21 S. L. Li, K. WaKabayashi, Y. Xu, S. Nakaharai, K. Komatsu, W. W. Li, Y. F. Lin, A. Aparecido-Ferreira and K. Tsukagoshi, *Nano Lett.*, 2013, **13**, 3546–3552.

22 S. Kim, A. Konar, W. S. Hwang, J. H. Lee, J. Lee, J. Yang, C. Jung, H. Kim, J. B. Yoo, J. Y. Choi, Y. W. Jin, S. Y. Lee, D. Jena, W. Choi and K. Kim, *Nat. Commun.*, 2012, **3**, 1011.

23 T. Cao, G. Wang, W. Han, H. Ye, C. Zhu, J. Shi, Q. Niu, P. Tan, E. Wang, B. Liu and J. Feng, *Nat. Commun.*, 2012, **3**, 887.

24 W. Zhao, R. M. Ribeiro, M. Toh, A. Carvalho, C. Kloc, A. H. Castro Neto and G. Eda, *Nano Lett.*, 2013, **13**, 5627–5634.

25 D. Li, R. Cheng, H. Zhou, C. Wang, A. Yin, Y. Chen, N. O. Weiss, Y. Huang and X. Duan, *Nat. Commun.*, 2015, **6**, 7509.

26 T. Yu and M. W. Wu, *Phys. Rev. B: Condens. Matter Mater. Phys.*, 2014, **90**, 035437.

27 S. Tongay, J. Zhou, C. Ataca, K. Lo, T. S. Matthews, J. Li, J. C. Grossman and J. Wu, *Nano Lett.*, 2012, **12**, 5576–5580.

28 K. P. O'Donnell and X. Chen, *Appl. Phys. Lett.*, 1991, **58**, 2924–2926.

29 J. S. Ross, S. Wu, H. Yu, N. J. Ghimire, A. M. Jones, G. Aivazian, J. Yan, D. G. Mandrus, D. Xiao, W. Yao and X. Xu, *Nat. Commun.*, 2013, **4**, 1474.

30 L. Yuan and L. Huang, *Nanoscale*, 2015, **7**, 7402.

31 G. Froehlicher, E. Lorchat and S. Berciaud, *Phys. Rev. B*, 2016, **94**, 085429.

32 Z. Jin, X. Li, J. T. Mullen and K. W. Kim, *Physics*, 2014, **90**, 55–58.

33 P. D. Cunningham, K. M. Mccreary and B. T. Jonker, *J. Phys. Chem. Lett.*, 2016, **7**, 5242.

34 A. Colev, C. Gherman, V. Mirovitskii, L. Kulyuk and E. Fortin, *J. Lumin.*, 2009, **129**, 1945–1947.

35 J. D. Yao, Z. Q. Zheng, J. M. Shao and G. W. Yang, *Nanoscale*, 2015, **7**, 14974–14981.

36 M. Palummo, M. Bernardi and J. C. Grossman, *Nano Lett.*, 2015, **15**, 2794.

37 H. Shi, R. Yan, S. Bertolazzi, J. Brivio, B. Gao, A. Kis, D. Jena, H. G. Xing and L. Huang, *ACS Nano*, 2013, **7**, 1072–1080.

38 M. K. Kwon, J. Y. Kim, B. H. Kim, I. K. Park, C. Y. Cho, C. C. Byeon and S. J. Park, *Adv. Mater.*, 2008, **20**, 1253–1257.

39 S. Tongay, J. Suh, C. Ataca, W. Fan, A. Luce, J. S. Kang, J. Liu, C. Ko, R. Raghunathanan and J. Zhou, *Sci. Rep.*, 2013, **3**, 2657.